Solid Freeform Fabrication 2021: Proceedings of the 32nd Annual International Solid Freeform Fabrication Symposium – An Additive Manufacturing Conference
Reviewed Paper

Laser Sintering Design Guidelines for media transmitting Components

I. Kletetzka*, C. Kummert*, H.-J. Schmid*

* Direct Manufacturing Research Center (DMRC) and Particle Technology Group, Paderborn University, Germany

Abstract

In automotive and other fields of application media transmitting components are made of plastics for reasons of weight and cost and complex, flow-optimized geometries are most desirable. Therefore, the laser sintering technology (SLS) is predestinated to manufacture these components as it offers a very high degree of design freedom and good mechanical properties. For industrial applications the long-term properties of the SLS material in contact with liquid media are important and were therefore investigated for polypropylene (PP) and polyamide (PA613). The mechanical properties were tested after immersion and compared to injection molded samples. Furthermore, laser sintering design guidelines for media transmitting components were developed. These guidelines for instance include the minimum wall thickness to ensure media tightness and strategies for the removal of powder from channels with a high length to diameter ratio.

Introduction

In recent years, selective laser sintering has evolved from a rapid prototyping technology to a suitable option for series production of sophisticated plastic components. In this context, the functional properties of additively manufactured components are becoming increasingly important [1]. In the scope of this work, the production of functional media-transmitting components by laser sintering is investigated in order to create guidelines for designers. Therefore, the effects of the laser sintering process on the media tightness and chemical resistance of the components are investigated. Furthermore, methods for increasing the maximum cleanable aspect ratio of fluid channels in laser sintered parts are developed.

State of the Art

As laser sintering materials are typically well known from conventional manufacturing methods, the chemical resistance and permeation coefficients are known as well. However, laser sintered parts have a higher crystallinity, rougher surfaces and show some porosity [2]. Therefore, the knowledge of conventional chemical material resistance and permeability should be validated.

There are two different mechanisms that determine the chemical resistance of polymers in media: physical and chemical interaction as defined by DIN 50035. Both interactions change the material properties and can lead to a deterioration of the service life and premature failure of plastic components. If the chemical structure of the macromolecules is changed, this is referred to as a chemical interaction. Examples are oxidation, hydrolysis, decomposition of the polymer chains or

depolymerization. These processes are not reversible. A reduction in the molecular weight of the macromolecules can severely reduce the mechanical properties of the plastic. [3, 4]

Physically interacting media do not react with the polymer. When a medium gets in contact with a plastic sorption of the medium on the surface takes place and it diffuses into the material. The diffusion process can be described by Fick's law and is influenced by the surface area and the crystallinity of the polymer. Inside the polymer, the media influences the secondary valence bonds in between the macromolecules of the polymer. This can lead to swelling or dissolution and changes in the crystallinity of the microstructure. All physical ageing processes can be reversed by remelting the polymer or removing the physically acting media from the polymer. [4]

The media tightness of an ideal polymer membrane without porosity can also be described with the model of solution diffusion. Therefore, the transport of molecules through a polymer layer is characterized by the adsorption and solution of the penetrating substance at the side of higher concentration, the diffusion in the polymer and the desorption on the side with the lower concentration. For this reason, the combination of chemical kinetics and sorption and solution equilibria has to be considered .The diffusion process is dependent on a gradient of concentration as described for the steady state in Fick's law (1). [4–6]

$$\mathrm{J} = -D \cdot \frac{\mathrm{dC}}{\mathrm{dx}} \tag{1}$$

Here, J is the flux through the specimen (transferred quantity per time and surface area). The correlation between the diffusion constant D and J is given in form of the concentration gradient dC/dx. The solubility of the diffusing substance in the polymer membrane directly impacts the concentration gradient in the membrane. [4–6]

However, SLS parts can not be regarded as ideal and homogenous polymer membranes. They show a characteristic porosity and defects that result from the layer-wise manufacturing process. The preheated powder is melted selectively with a CO2-laser to create the final part. The surrounding powder supports the melt pool and the process is pressure-less and relies on the coalescence of the polymer melt. This results in parts with a characteristic surface roughness and porosity inside the parts. The porosity is heavily influenced by the process parameters, for example an insufficient energy density of the laser leads to partly unmolten particles in the parts. A typical part porosity for well-adjusted build parameters is in between 3% and 5%. [2, 7]

The different types of porosity that can occur with SLS parts are illustrated by figure 1. Closed and blind pores have limited effect on the permeability of the part. The model of solution diffusion can still be used for describing the transportation of the permeate. In case of blind pores, the effective material thickness is lowered and in case of closed pores there are multiple absorption, diffusion and desorption processes within the pore that contribute to the total permeability. Through-pores have a significant impact on the permeability of the part. If the part contains through-pores, the permeability regarding pressure differences can be modeled with fluid dynamics instead of solution-diffusion. The permeability of a polymer membrane with through holes will be magnitudes higher than the diffusion driven permeability. Through holes in SLS parts occur mostly with thin wall thicknesses because single defects in the melt pool can directly lead to channels. If

the wall thickness is higher, than the through hole of the first layer is often closed off by the melt pool of the following layers so that blind pores or closed pores are generated. [8]

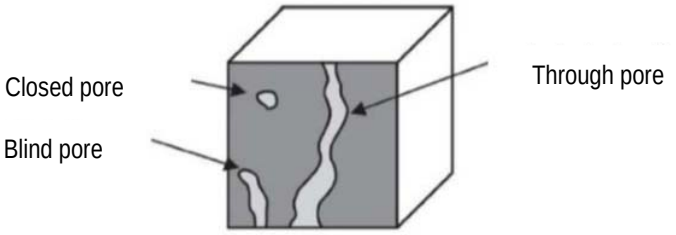

Figure 1: Different types of pores [8]

Another important factor for laser sintering of fluid transmitting parts is the removal of remaining powder after the build job is finished. Since the powder cake is preheated close to the melting point, it starts to fuse together. This can create difficulties when trying to remove the powder from fluid channels. In Adam, it was found that the cleanable length of fluid channels increases almost linear with the diameter when cleaning the channels with compressed air [9]. Furthermore, Adam reported, that the maximum cleanable length is five times the diameter for straight channels when using compressed air with a pressure of 4 bars and blowing out the channel from one side [9]. In order to overcome these limitations, methods for cleaning fluid channels with higher aspect ratios and the effect of curved fluid channels will be analyzed.

Experimental Methods

Chemical Resistance

To determine the behavior of the LS samples against liquid chemicals, tests according to DIN EN ISO 175 are performed. The test specimens are completely immersed in a test medium for a specified duration and at a specified temperature [10]. The mass, dimensions, appearance and mechanical properties are determined before and after exposure to the medium. For each test point (temperature-time combination) 5 tensile (DIN EN ISO 527-2) and 5 Charpy (DIN EN ISO 179) specimens are tested and evaluated. Further, the initial values of the tensile and Charpy impact properties are determined according to the corresponding International Standards [11, 12]. Before testing the mechanical properties, all test specimens are rinsed, wiped dry and stored at standard climate (23°C, 50 % humidity) for 24 hours.

Table 1: Test media, Testing temperatures and test specimen materials

	Glysantin G40 coolant [13] (50:50 mix with water)	Engine Oil [14] (Divinol Spezialöl HGB)
PP (Ultrasint PP nat 01) [15] Laser sintered	-40°C / 23°C / 90°C	23°C / 90°C
PA613 (VESTOSINT 3D 8754 HT1) [16] Laser sintered	-40°C / 23°C / 90°C / 103°C	-25°C / 23°C / 90°C / 150°C
PA613 (VESTOSINT 3D 8754 HT1) Injection molded	-40°C / 23°C / 103°C	-25°C / 23°C / 90°C / 150°C

Media Tightness

There are various different standards for determining leakages and permeation coefficients. Since the results of this research should be applicable to pressurized media transmitting parts the test methods of different standards were combined. The testing method pressure loss monitoring according to DIN EN 1779 was chosen as the basic principle for measuring the leakage. A test object is pressurized and then closed off. The pressure loss over a time period is measured to quantify the media tightness of the system [17]. However, this standard is only applicable to test objects that can be closed off and have an internal volume. To allow the use of simple test specimens, parts of the DIN 53380-2 standard were used in addition. DIN 53380-2 specifies the determination of gas permeability of plastic films with the manometric method [18].

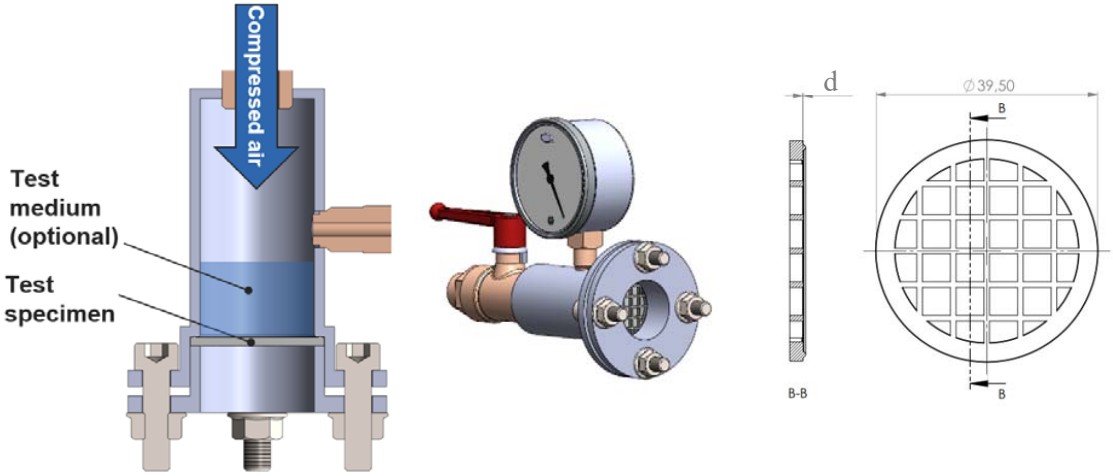

Figure 2: Test setup for examining media tightness of SLS test specimens

The main component of the test setup is a pressure chamber that can be closed with a ball valve (figure 2). The pressure inside the chamber is monitored with a digital manometer with a resolution of 0,02 bar. For verification purposes there is an additional analogue manometer installed. Furthermore, the temperature of the pressure chamber is monitored with a thermocouple. Test specimens can be clamped against the pressure chamber with a clamping ring and four bolts. The tension in the bolts is selected high enough to plasticly deform the sealing surface of the test specimens. This ensures the best possible seal. After the test setup has been pressurized the ball valve is closed. Pressure and temperature are monitored and one data point per second is generated. Since the volume of the pressure chamber is known, the leakage flow can be calculated from the pressure loss utilizing the ideal gas law. The test duration was varied based on the leakage flow.

All media tightness test specimens were built on an EOS P396 using EOSINT PA 2200 polyamide 12 powder with a 50% recycling rate. The layer height for all test specimens was set to 120 µm and standard EOS balance parameters were used. The geometry of the test specimens is shown in figure 2. The nominal wall thickness d of the specimens was varied in between 0,12 mm and 2,4 mm. The thin sintered membrane was reinforced with a grid to limit the deformation. Tests were conducted with water as an additional test medium and with compressed air only.

Depowdering analyzes

For the depowdering investigations, two different sample geometries have been developed. The first sample is used for analyzing the cleaning behavior of straight fluid channels with different diameters. The second specimen has a 180° bend. This specimen is used to analyze the effects of curves that will often occur in real applications. The radius of the 180° bend is three times the inner radius of the fluid channel. All specimens are manufactured on an EOS P396 machine using PA 2200 powder, a layer height of 120 µm and the standard EOS balance parameter set.

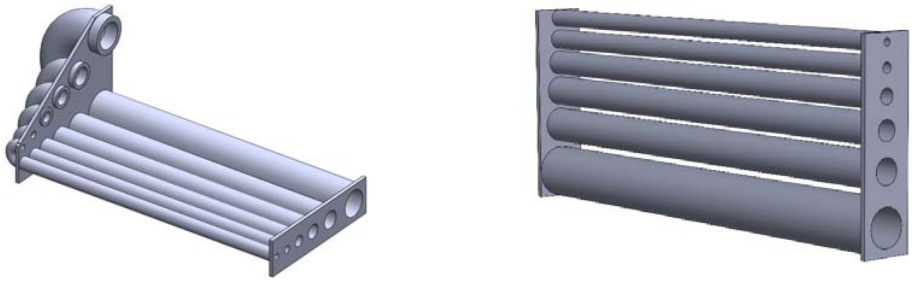

Figure 3: Geometry of the test specimens used for depowdering analyses

Table 2: Depowdering test specimens

Specimen type	inner diameter of the fluid channels [mm]	Wall thickness [mm]	total length of the fluid channel [mm]
straight	1,5, / 2 / 3 / 4 / 5 / 7,5	1,0	100
	10 / 12,5 / 15 / 20 / 25	1,5	250
180°-curve	1,5, / 2 / 3 / 4 / 5 / 7,5	1,0	88 / 90 / 96 / 101 / 106 / 119
	10 / 12,5 / 15 / 20 / 25	1,5	252 / 265 / 278 / 304 / 330

The standard cleaning method is to blow out the powder from inside the fluid channels with compressed air. The fluid channels were cleaned only from one side (in case of the specimens with the 180° curve, cleaning was done from the curved side). The specimens were blasted with compressed air, until no more powder could be removed from inside the fluid channels. Different pressures and nozzle sizes were tested. An air gun with a small nozzle was tested with pressures of 4 and 8 bars. A different air gun with a bigger nozzle was tested with a pressure of 10 bars. After cleaning, the free length was measured by shining a bright light through the test sample

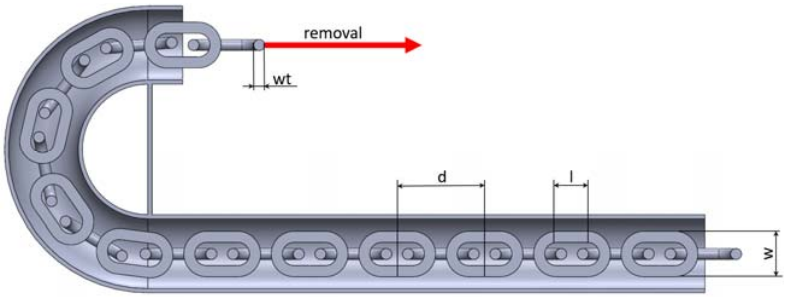

Figure 4: Depowdering chain in curved fluid channel

An approach for cleaning channels with a higher aspect ratio is, to build chains or strings together with the part and pulling them out in order to assist the cleaning process with compressed

air. Pulling out the chains or strings from inside the fluid channel generates an initial through hole for further cleaning the part with compressed air. Since it is much more effective to clean a through-hole with compressed air than cleaning a blind hole, this method is promising for cleaning fluid channels with a higher aspect ratio. For chains the idea is, that the chain stretches out while it is removed so that every chain link breaks free individually. Furthermore, the chain should provide the necessary flexibility to be removed from curved channels. Chains were tested for hole diameters of 10 mm up to 25 mm. For smaller diameters, strings were used since the chain links would be too fragile. However, it is expected that the limited flexibility of the strings will make the removal more difficult with curved fluid channels.

Results and discussion

Chemical Resistance

In figure 5 the mechanical properties of LS PP after immersion in Glysantin coolant are shown. Polypropylene is a polyolefin, therefore the behavior towards chemicals is determined by the non-polar character. The different color shades illustrate different storage temperatures.

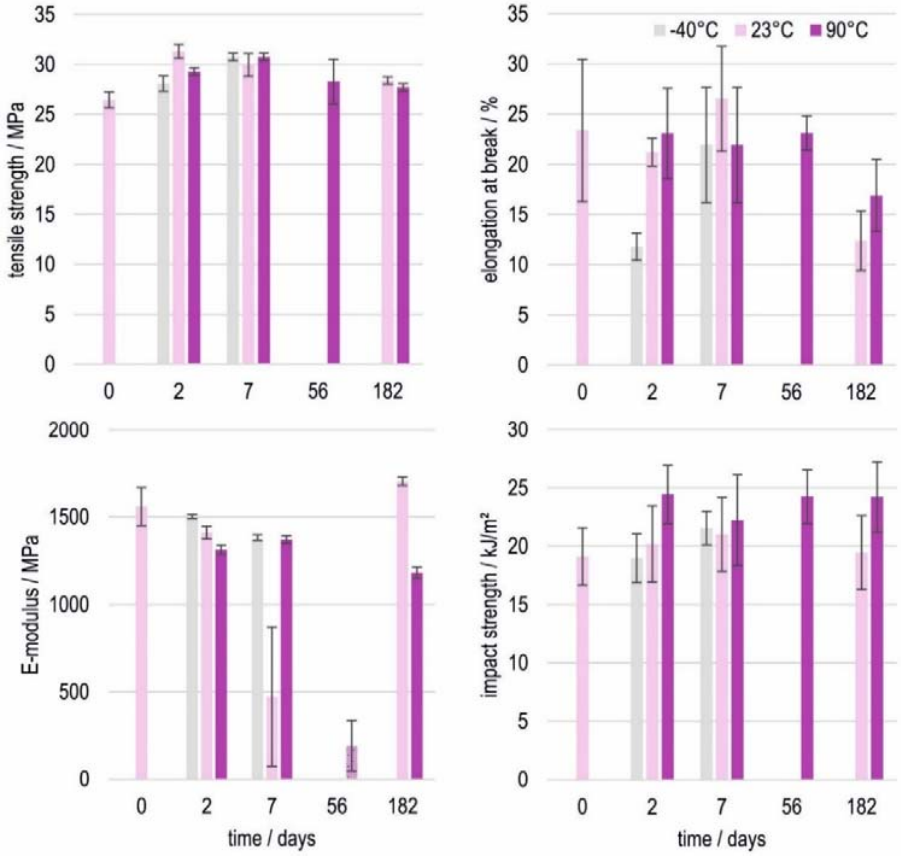

Figure 5: Mechanical Properties of LS PP after immersion in a coolant (Glysantin G40)

Storage of the specimens in Glysantin at low temperatures (-40°C and 23°C) leads to a slight increase of tensile strength. Also, after immersion at 90°C a slight increase is observable but is reduced to the initial value after 182 days storage. The elongation at break shows even in an untreated stage a high standard deviation, so that the high fluctuations cannot be clearly assigned to immersion in the medium. Again, the changes in E-modulus show no decisive trend. The low value after 56 days at 90°C can be clearly assigned to a measurement problem of the testing machine. Only the Charpy impact strength after immersion at 90°C seems to be increased over the entire storage period.

The PP specimens showed no significant changes in mass or volume after immersion and no mass reduction after the drying process. Therefore, it can be concluded that no swelling occurred. Regarding the mechanical properties as well as the mass changes, it can be stated that LS PP is not affected significantly by immersion in the coolant within the investigated temperature and time range. These results are in line with literature on injection molded components [4].

The next medium which is investigated in contact with LS PP is an engine oil. In figure 6 the resulting mechanical properties are shown. Here, clear trends are observable. For immersion at 23°C tensile strength is not affected, but the elongation at break decreases over time whereas the E-modulus and impact strength are slightly increased. Immersion at 90°C significantly increases the elongation at break up to 56 days, before it starts dropping off again. The E-modulus is reduced to under 500 MPa and the tensile strength is slightly decreased.

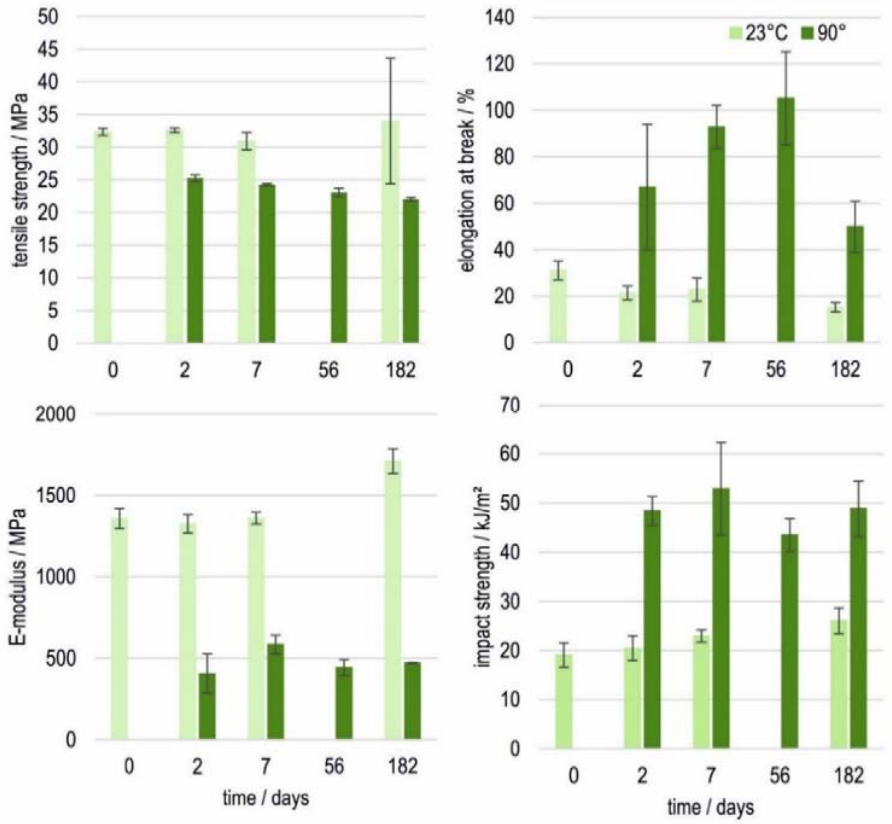

Figure 6: Mechanical properties of LS PP after immersion in an engine oil

The specimens stored in engine oil at 90°C for two days showed an increase in weight of 40%. However, the weight increase lowered for longer storage times. After 182 days of storage almost no increase was measurable when compared to the starting values. For immersion at 23°C the mass was slowly increasing with the immersion time. These effects might indicate, that the dominating effect at elevated temperatures and short immersion times is swelling. However, after extended immersion a chemical interaction or dissolution might cause a loss in weight. Injection molded PP also swells in aliphatic hydrocarbons, as it was observed for LS PP here [4].

The next material under investigation is PA613 which is a polyamide and therefore shows, in contrast to PP, a polar chemical behavior. The mechanical behavior of PA613 after immersion in the coolant Glysantin is shown in figure 7. Immersion at room temperature has only a low influence on the tensile strength. Higher temperatures (90°C and 103°C) lead to a more obvious reduction in tensile strength. Elongation at break on the other side is slightly increased for these temperatures up to 7 days. The E-modulus is also decreasing for all temperatures up to 7days. Surprisingly, after 182 days at 23°C the highest value is reached. Further, the Charpy impact strength shows no decisive trend.

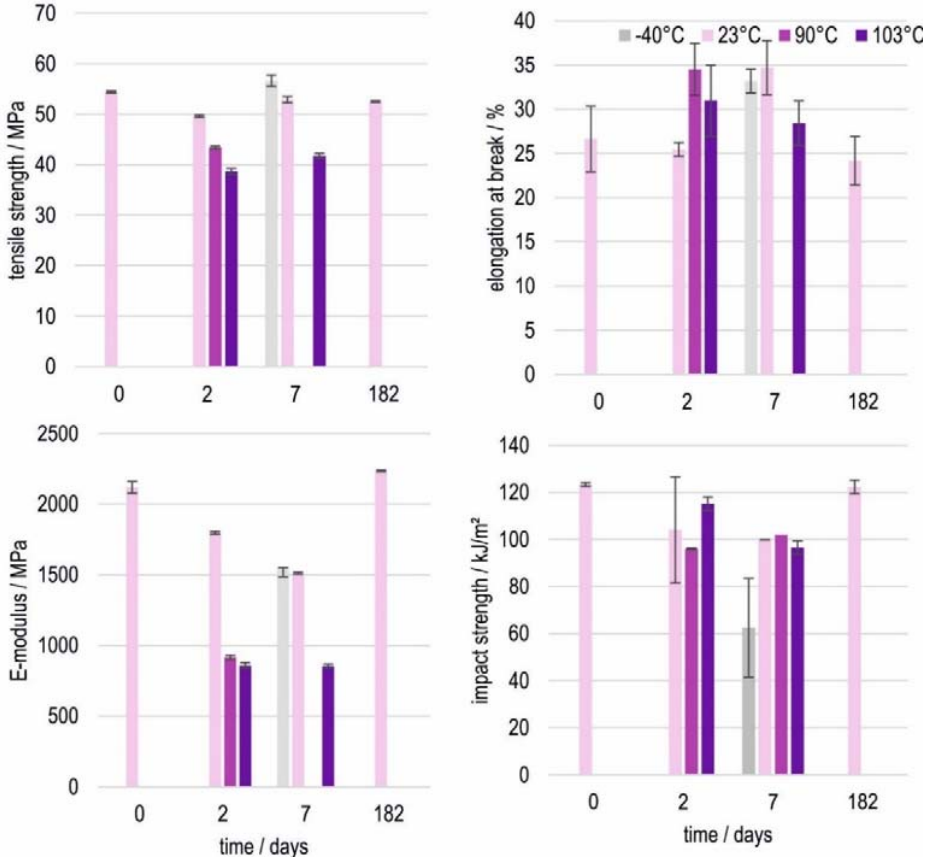

Figure 7: Mechanical properties of LS PA613 after immersion in a coolant (Glysantin G40)

When PA613 is stored in a Glysantin water mix at room temperature, the mass increases slowly over time reaching a 1% increase after 182 days. When stored at 103°C a 5% increase is

reached after 2 days and is constant for longer immersion times. These findings combined with the mechanical properties indicate swelling of the specimens.

Storing PA613 in engine oil at elevated temperatures decreases the elongation at break as shown in figure 8. The tensile strength remains constant even for elevated temperatures and duration up to 182 days. The E-modulus decreases to around 1500 MPa for all tested temperatures, but increases again at 182 days immersion time. The impact strength decreases for all specimens, the effect is the strongest at elevated temperatures. A small increase in mass of up to 1% occurs at elevated temperatures and longer immersion times.

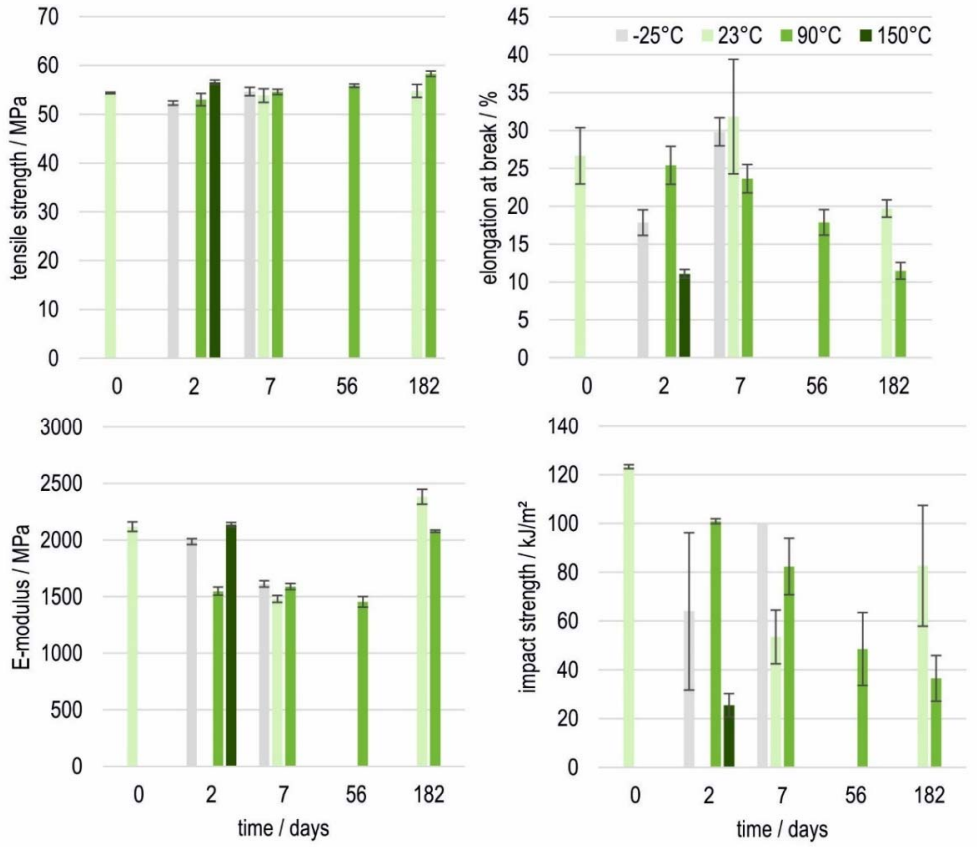

Figure 8: Mechanical properties of LS PA613 after immersion in an engine oil

Since there is no literature available on PA613 injection molded specimens were made from the Vestosint PA613 powder and immersed in a glycol water mixture and engine oil. The results for laser sintered and injection molded specimens are compared in figure 9 and 10.

It is clearly visible that IM PA613 has higher elongation at break than LS. However, the standard deviation is quite high which might be due to the process of IM in the laboratory which needs improvement. But as PA613 is a material tailored for the laser sintering process IM parameters are not known. Looking at the tensile strength, the initial values for IM and LS PA613 are almost identical. Furthermore, the values after immersion in engine oil or coolant behave very similar. The initial value of the E-modulus of IM PA613 is slightly lower, however immersing the

specimens in test media had the same effects on IM and LS parts. Both showed a strong decrease for immersion in Glysantin based coolant at 103°C. The elongation at break of IM and LS parts show the same trends after immersion, but the high standard deviation makes it difficult to make precise statements. For immersion in engine oil at 150°C, the elongation at break is strongly reduced for both samples.

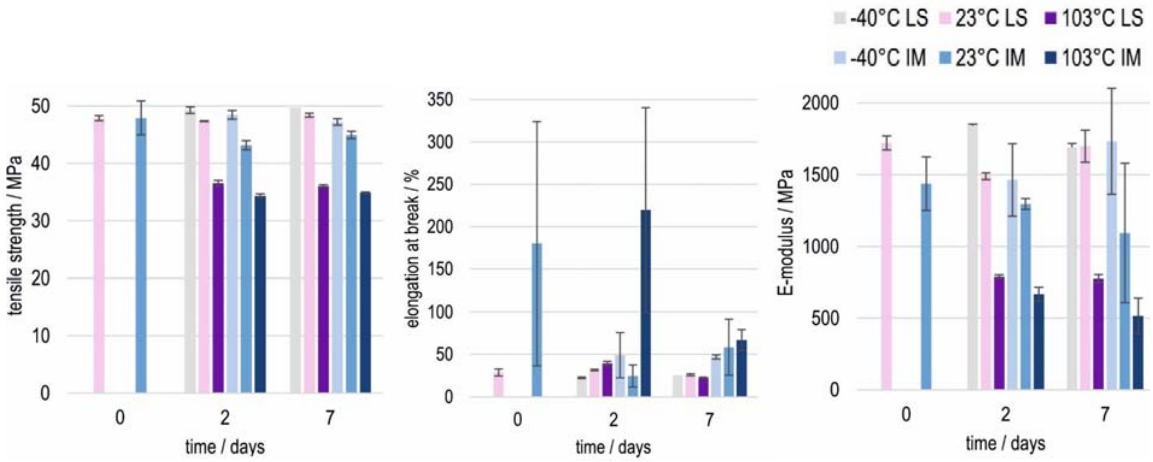

Figure 9: Laser sintered and injections molded PA613 after immersion in a coolant (Glysantin)

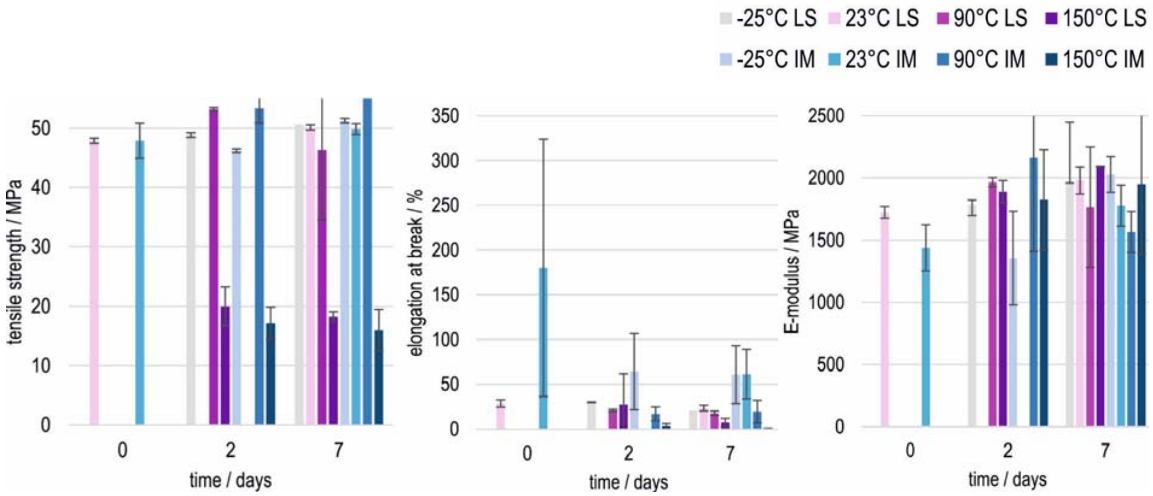

Figure 10: Laser sintered and injections molded PA613 after immersion in an engine oil

It can be concluded, that the behavior of a polymer in contact with a fluid media is primarily determined by the combination of the polymer, the type of media, the temperature and the immersion time. The tests with PA613 have shown that the manufacturing process plays only a minor role. A good indicator for predicting the physical interactions between the plastic and the medium is the polarity. Polar plastics such as polyamides tend to swell, especially in polar media such as water. In contrast, non-polar plastics such as polypropylene tend to swell in non-polar media such as oils.

Media Tightness

The method for calculating the normalized leakage flow from the pressure loss for tests with compressed air only is exemplary explained for the results of sample P21. Figure 10 shows the recorded pressure loss over the test duration. The pressure los was approximately 0,05 bars in 50 hours. However, the information is not very useful for designers of media carrying parts, because it is only valid for the volume of the pressure chamber that was used for testing and the given specimen geometry. For this reason, the air mass m_{air} is calculated from the pressure inside the chamber using the ideal gas law:

$$m_{air} = \frac{p * V_{chamber}}{R_s * T}$$

The mass of air is proportional to the pressure p and the volume of the pressure chamber $V_{chamber}$ and anti-proportional to the temperature T and the gas constant $R_s$of air. The volume of the pressure chamber is 73 ml. The resulting graph for the air mass is shown in figure 10.

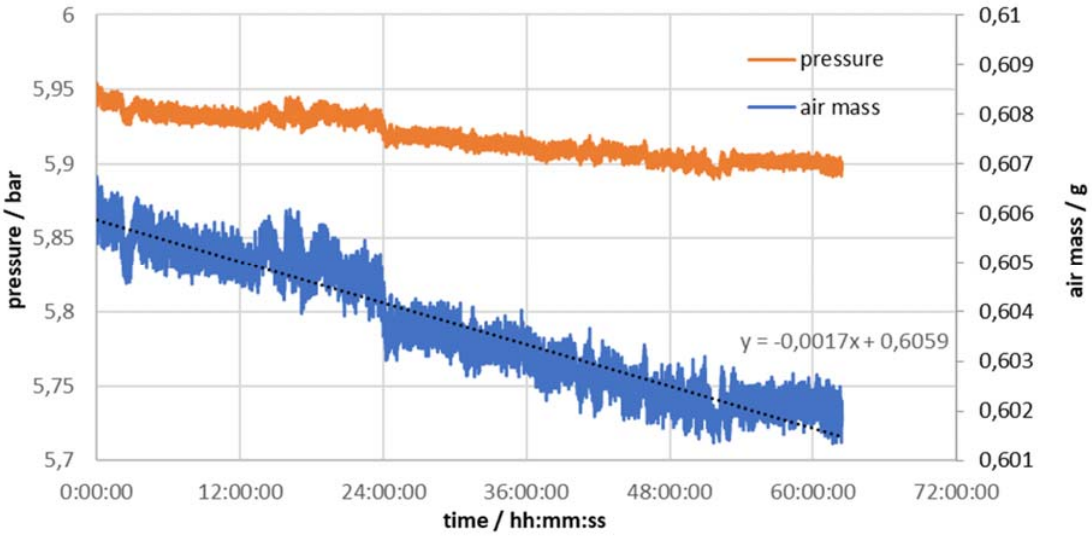

Figure 10: measured pressure and calculated air mass inside the pressure chamber for P21 (0,36 mm nominal wall thickness and 0° building orientation – test with compressed air only)

A linear regression can be fitted in order to calculate the leakage flow for the given pressure level. In case of test specimen P21 the leakage flow is

$$\dot{m}_{P21} = 0{,}0017\ \frac{g}{d}$$

This value can be normalized by accounting for the surface area of the polymer membrane and the test pressure. The surface of the specimens is 586,4 mm² and the mean pressure during the test was 5,925 bars. Therefore, the normalized leakage flow for P21 is:

$$\dot{m}_{norm,P21} = 0{,}0014\ \frac{g}{m^2 * bar * h}$$

This method is used for calculating the leakage for all specimens tested with compressed air. The normalized leakage flow of the specimens is plotted against their nominal wall thickness. The data is evaluated separately for the different building orientations of the specimens. Figure 11 shows the normalized leakage flow for all test specimens which were tested with compressed air.

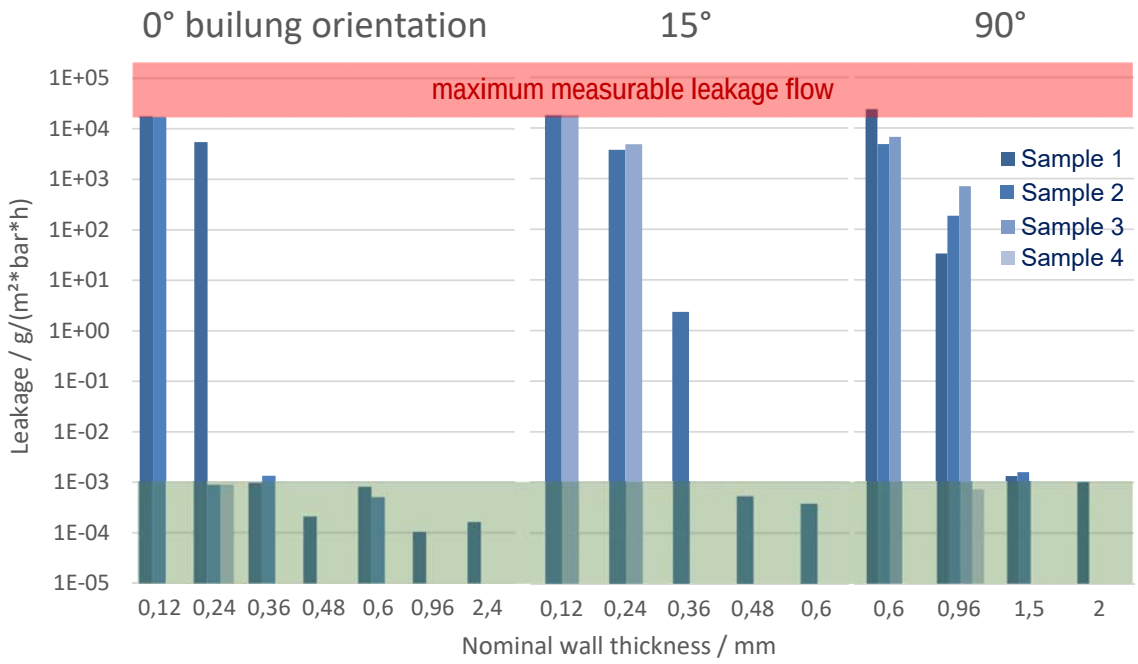

Figure 11: normalized leakage flow for all tests with compressed air

The leakage flow is plotted in dependence on the nominal specimen thickness and the build direction. A logarithmic scale is used. For a given build direction, the leakage flow decreases with increased wall thicknesses. For small wall thicknesses, the leakage flow is very high, due to defects (through-pores) of the test specimens. With increasing wall thickness, the media tightness improves significantly at first. For higher wall thicknesses, the specimens do not contain any through pores and the leakage flow can therefore be modelled with solution-diffusion. The diffusion rate is expected to be anti-proportional to the wall thickness due to the Fick model. Therefore, at walls consisting of at least 3-5 layers the leakage is not as significant as for low wall thicknesses.

In addition to the wall thickness, the building orientation in the sintering process has a significant influence on the media tightness. Specimens, that are built in the XY plane show the best media tightness for thin wall thicknesses, while specimens built in a 90° orientation to the building platform perform the worst. This can be explained with the layer-wise construction of the test specimens. A specimen, built in 90° orientation, consists of multiple layers with small cross sections. These layers have to fuse together perfectly in order for the specimens to be media tight. A test specimen with a nominal wall thickness of 0,12 mm which is built in the XY plane only consist of a single layer. Therefore, the specimen would be media tight, if the powder within one layer would fuse together perfectly, the bond between layers is not critical.

It can be concluded that the minimum advisable wall thickness depends on the building orientation. The threshold for an acceptable tightness is defined as the transition from defect driven permeation to diffusion within this work. Samples built in the XY plane showed a good media tightness for nominal wall thicknesses of 0,36 mm, i.e. 3 layers, or higher. Samples built at an angle of 15° achieved a good media tightness for wall thicknesses of 0,48 mm or higher while samples built in 90° orientation required a minimum of 1,5 mm. It should be noted, that these values are only applicable for an EOS P3-system using PA2200 and a layer height of 120 µm and standard EOS balance parameters. The effect of different laser parameters and scan strategies should be investigated in further research. Due to the long duration of the permeation tests, only a limited number of tests could be carried out, therefore the results are not statistically validated.

Figure 12 shows the leakage flow of the test specimens which were tested with water inside the pressure chamber and a test pressure of 6 bars. The qualitative results are consistent with the test with compressed air. The quantitative results differ, because of the differences in viscosity, density and solubility. As explained for the test with air, the leakage flow is dependent on the wall thickness and the building orientation. The best results are again achieved with specimens built in the XY-plan and the worst with specimens built in a 90° angle in relation to the XY-plane of the sintering machine. All test specimens with a wall thickness of 0,24 mm or lower show a high leakage rate due to defects such as through pores in the membrane. The minimum advisable wall thickness for water carrying parts is the same as for pneumatic components since through-pores have to be avoided for all media-carrying parts

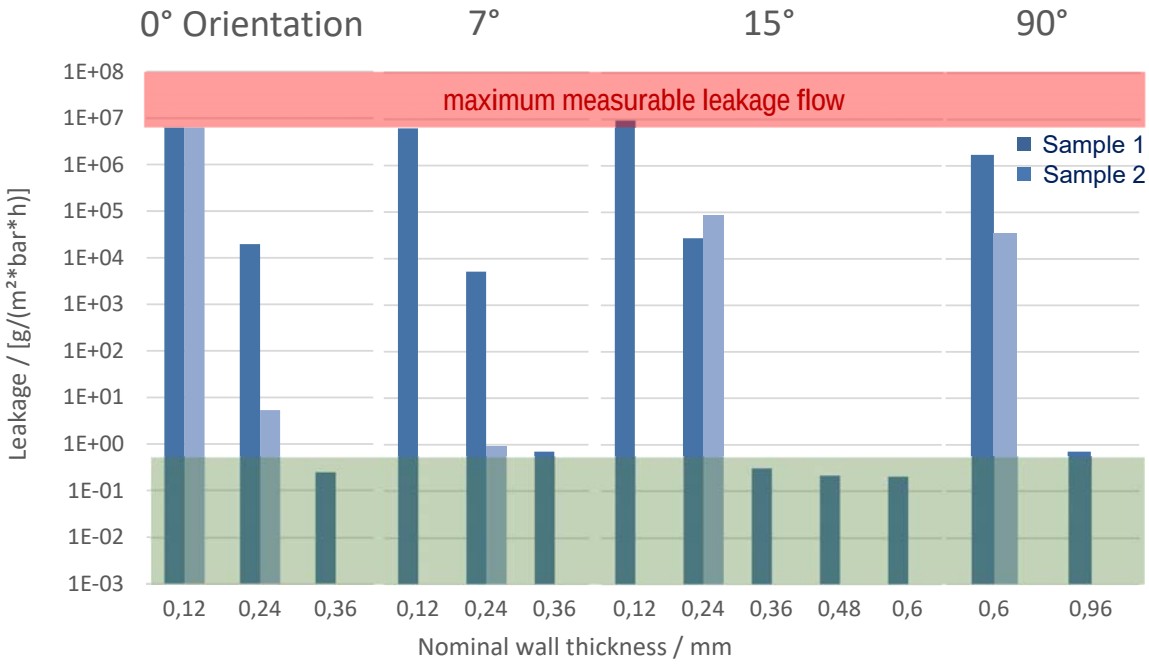

Figure 12: normalized leakage flow for all tests with water inside the pressure chamber

As the water was colorized with ink before the test, the defects of the test specimens were visible after testing as illustrated by figure 13. The visible defects correlate nicely with the

measured leakage flow of the samples. Specimens P62 and P511 show visible through-pores, were the pressurized test medium could escape quickly. While the sample that was built in 90° orientation shows considerable number of smaller defects, the sample built in 15° orientation shows only two major defects. Diffusion does not have a significant influence for these specimens, because the leakage from the through pores is magnitudes higher. Test Specimen P531 shows no visible defects and the measured leakage flow is much lower. The water has been transmitted through the entire surface of the test specimen.

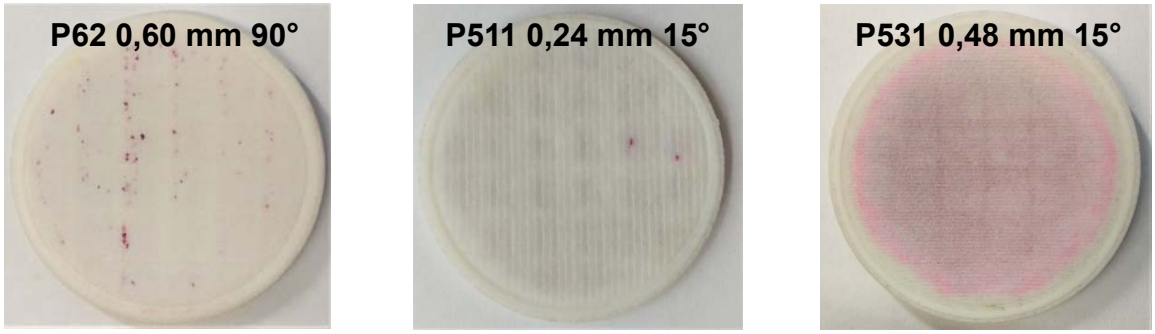

$\dot{m} = 35578\ \frac{g}{m^2 * bar * h}$ $\dot{m} = 27597 \frac{g}{m^2 * bar * h}$ $\dot{m} = 0{,}2153\ \frac{g}{m^2 * bar * h}$

Figure 13: visible defects after testing with pink colored water

After determining the media tightness of as built laser sintered samples, further tests with samples were carried out, which were treated with a chemical surface smoothing process in order to improve their media tightness. The chemical surface smoothing process affects the bonds between the polymer chains. These are connected in thermoplastic polymers via hydrogen bonds and van der Waals forces but are not chemically crosslinked. The part is inserted in a heated process chamber with solvent vapors. The polar solvent vapor condenses on the surface of the components and dissolves these bonds. Due to the thermodynamic tendency to minimize the surface energy and thus the total surface, the molecular chains rearrange themselves. This process results in a smoothing of the surface. As a side effect small pores in the surface are closed off during the process. At the end, the solvent is removed from the parts by vacuum drying. The company DyeMansion offers chemical surface smoothing as a service under the trade name “VAPORFUSE SURFACING” (VFS). The company advertises that their VFS technology will not only reduce the surface roughness but furthermore create media tight parts that are easy to clean. [19]

The surface roughness can be significantly lowered by the VFS treatment. The untreated samples have a typical surface structure of SLS parts that is characterized by partly molten powder particles and stair stepping in case of the 15° building orientation. The treated samples show a uniform and glossy finish. The stair stepping effect for the 15° building orientation was considerably reduced, but is still noticeable. It has to be noted, that the vapor fuse surfacing process cause the samples to warp slightly. Samples with a very low wall thickness showed more significant warpage than samples with a higher wall thickness. However, the warpage did not influence the functionality of the samples and all samples still fitted inside the test setup.

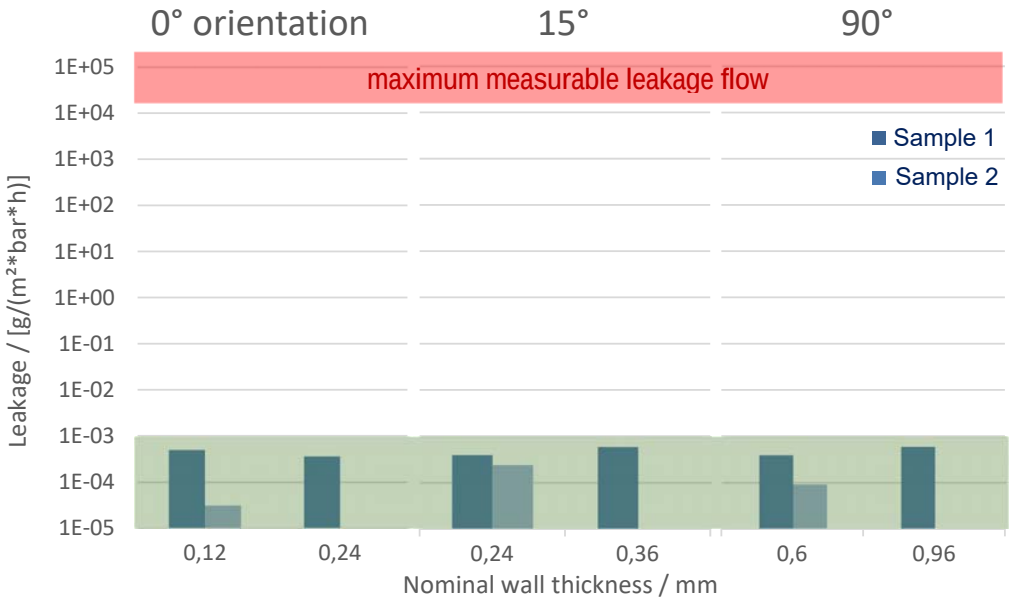

Figure 14: normalized leakage flow for test specimens treated with VFS

The test specimens which were treated with the chemical surface smoothing were afterwards tested with compressed air. The same test parameters were used as for the untreated samples. The results of the treated samples are summed up in figure 14. The leakage flow of all treated samples was below the previously determined threshold for good media tightness. The chemical smoothing process closed all through-pores, so that even the sample with a nominal wall thickness of 0,12 mm which consists only of one layer showed good media tightness. Before all samples with a wall thickness of 0,12 mm showed a very high leakage flow and a high number of through-pores. The minimum advisable nominal wall thickness can therefore be reduced to 0,12 mm for parts build in the XY-plan, 0,24 mm for parts built at an angle of 15° and 0,6 mm for parts built at 90°. It can be concluded that the vapor fuse technology from DyeMansion can be used to significantly improve the media tight-ness of parts with a very low wall thickness. If the parts are constructed with a wall thickness of 1,5 mm or higher to achieve the desired strength or stiffness, vapor fuse surfacing is not necessary to achieve a good media tightness.

Depowdering analyzes

After testing all the different cleaning methods, the powder free length was measured for every test specimen. The results for the straight fluid channels are shown in figure 15. After the strings or chains were removed, some loose powder remained in the channels. However, this powder was easily removable with compressed air. Therefore, the cleanable length for the specimens was equal to the specimen length, if the chain or string could be pulled out without breaking. If the chains or strings snapped during removal the cleanable length was assumed to be 0 mm for this sample.

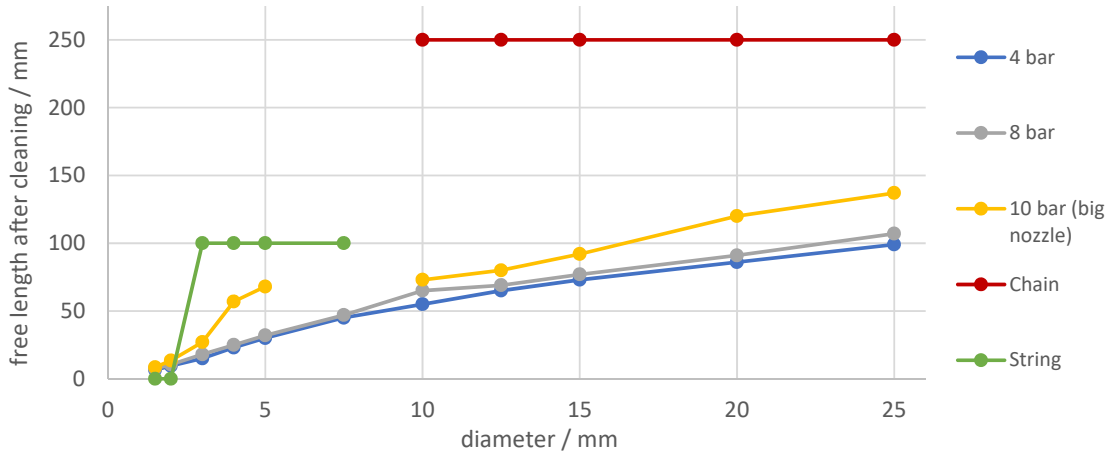

Figure 15: Depowdering of straight fluid channels – free length after cleaning

The results for cleaning the straight fluid channels with compressed air with a pressure of 4 bars are generally similar to the findings of Adam [9]. However, small fluid channels showed a higher cleanable aspect ratio than in Adams research. This might be due to differences in the nozzle of the air gun or the temperature control of the laser sintering machine. The cleanable length increases almost linear with the inner diameter of the channel. The cleanable length to diameter ratio is therefore nearly constant when cleaning the samples with the small air gun. The maximum cleanable aspect ratio of around 6 is achieved for channels with a diameter in between 4 and 7,5 mm. For bigger channels the cleanable aspect ratios decreases slightly to around 4,5 for fluid channels with a diameter of 25 mm. Increasing the air pressure to 8 bars showed very little effect when using the same air gun. Using an air gun with a bigger nozzle and an air pressure of 10 bars improved the cleanable aspect ratio noticeably for fluid channels with an inner diameter of 3 mm and higher. Channels with an inner diameter of 3 and 4 mm showed a cleanable aspect ratio of 14. Channels with an inner diameter of 10 mm and higher had a cleanable aspect ratio of around 6, which is still higher than in previous tests, but the improvement is much smaller.

All chains could be removed without breaking, therefore the cleanable length for the fluid channels ranging from 10 mm up to 25 mm is 250 mm. Even higher lengths might be possible but were not tested. This results in a maximum tested aspect ratio of 25 for fluid channels with an inner diameter of 10 mm. For this sample, the tested cleanable length is almost 4 times greater than with compressed air. Since the specimen length was kept constant for 10 mm - 25 mm diameter, the tested cleanable ratio decreases with larger diameters. An aspect ratio 25 or higher might also be possible for straight fluid channels with larger diameters, but was not tested because of the limited build area of the used EOS P396 system.

The strings in holes with an inner diameter of 1,5 mm and 2 mm could not be removed. The clearance in between the string and the inner diameter was too small which caused the string to partly fuse to the channel. The strings snapped when trying to remove them. All strings in channels with an inner radius of 3 mm and larger could be removed from the samples with a length of 100 mm. This results in a maximum tested cleanable aspect ratio of 33 for channels with an inner diameter of 3 mm. The cleanable length is more than six times higher when compared to the results

with compressed air and a pressure of 4 bars. As already explained for the depowdering chains, the maximum aspect ratio was not determined, since all tested samples had the same length. However, it can be stated that the cleanable aspect ratio of straight fluid channels ca be increased significantly by utilizing depowdering chains or strings.

The free length of the curved fluid channels after cleaning is shown in figure 16. For depowdering with compressed air, the free length of the curved fluid channels increases approximately linearly with the diameter of the channels for cleaning with compressed air. The cleanable aspect ratio is slightly reduced in comparison with straight fluid channels. With an air pressure of 4 bars and the small nozzle size, the maximum cleanable aspect ratio is 4.9 for 10 mm channels. The ratio decreases to 3,6 for an inner diameter of 25 mm. Therefore, the cleanable aspect ratio is reduced by around 20% for curved channels in comparison to straight fluid channels. The cleanable length for compressed air with 8 bars and 10 bars with a bigger nozzle size is also reduced when compared to straight channels. Especially for channels up to 10 mm diameter, the cleanable aspect ratio is significantly lower with 10 bars. For bigger inner diameters, the difference is around 10 % and therefore less significant.

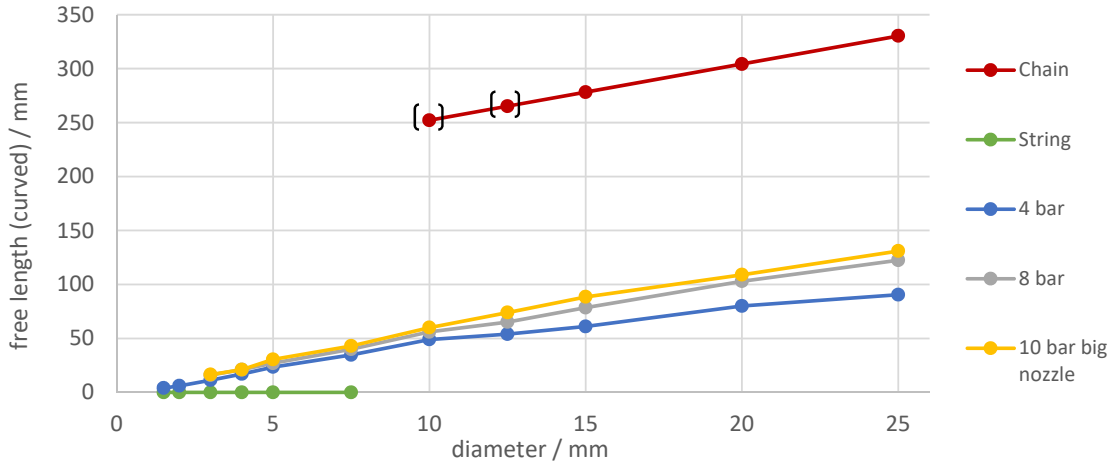

Figure 16: Depowdering of curved fluid channels – free length after cleaning

The chains inside the channels with a diameter of 15 mm – 25 mm could be removed by pulling them around the 180° bend as shown in figure 4. For the diameters of 10 mm and 12,5 mm, the chains snapped in the removal process. If the chains were pulled from the other side, they could be removed without breaking. The use of depowdering strings is not feasible for bent fluid channels. None of the strings could be removed from the test specimens. For the smaller diameters the strings snapped off and for the larger diameters the strings were so stiff that they could not be removed at all.

It can be concluded that chains and strings are an effective way to extend the cleanable length of fluid channels. If the channels shall be cleaned with compressed air, an aspect ratio of around 5 is a good starting point for fluid channels that can only be accessed from one side. If the fluid channel can be cleaned from both sides the cleanable aspect ratio can be doubled. If a higher aspect ratio is needed, depowdering chains and strings can be utilized. However, strings can only be used for straight fluid channels.

Summary

The investigations have shown that laser sintered components can be successfully used as media transmitting components, as long as certain design guidelines are adhered to. First of all, the chemical resistance of the polymer against the media has to be considered. The investigations showed, that laser sintered samples exhibited similar media resistance to injection molded samples, despite the differences in the part microstructure. The behavior of a polymer in contact with a fluid media is primarily determined by the combination of the polymer, the type of media, the temperature and the immersion time. Therefore, the laser sintering material has to be chosen with regard to the application and media.

Furthermore, the media tightness of laser sintered test samples has been investigated. It has been found that the orientation of the specimens in the build process, in addition to the thickness of the specimens, has a strong influence on the media tightness. Samples built in the XY plane exhibited a good media tightness for nominal wall thicknesses of 0,36 mm or higher. Samples built at an angle of 15° showed a good media tightness for wall thicknesses of 0,48 mm or higher while samples built in 90° orientation required a minimum wall thickness of 1,5 mm. Further tests with samples treated with a chemical surface smoothing process demonstrated, that the media tightness can be greatly improved with the tested VFS technology.

Another aspect that must be considered when designing media transmitting SLS-components is the depowdering of channels with a high length-to-diameter ratio. Since the powder cake is preheated close to the melting point of the polymer, it starts to fuse together. Thus, it can be challenging to remove powder from long fluid channels with a small diameter. When cleaning the channels from one side with compressed air, with a pressure of 8 bars, the maximum cleanable aspect ratio (length/diameter) was around 6 for all tested diameters. This ratio could be improved significantly by building chains or strings together with the part and pulling them out during post processing to assist depowdering with compressed air.

References

[1] M. Schmid, *Selektives Lasersintern (SLS) mit Kunststoffen*. München: Hanser, 2015.

[2] M. Blattmeier, *Strukturanalyse von lasergesinterten Schichtverbunden mit werkstoffmechanischen Methoden*. Wiesbaden: Vieweg+Teubner Verlag, 2012.

[3] *Begriffe auf dem Gebiet der Alterung von Materialien - Polymere Werkstoffe*, 50035, DIN, Berlin, 2012.

[4] G. W. Ehrenstein and S. Pongratz, *Beständigkeit von Kunststoffen*. München: Hanser, 2007. [Online]. Available: http://deposit.dnb.de/cgi-bin/dokserv?id=2799749&prov=M&dok_var=1&dok_ext=htm

[5] G. S. Park, "Transport Principles—Solution, Diffusion and Permeation in Polymer Membranes," in *Synthetic Membranes: Science, Engineering and Applications*, P. M. Bungay, H. K. Lonsdale, and M. N. Pinho, Eds., Dordrecht: Springer Netherlands, 1986, pp. 57–107.

[6] R. M. Barrer, *Diffusion in and through solids*. Cambridge: Cambride University Press, 1941. [Online]. Available: https://books.google.de/books?hl=de&lr=&id=npkWAwAAQBAJ&oi=

fnd&pg=PR11&ots=QtGA8AIXFt&sig=HCBuX-t8oBbIKqD4CNUPYNJpzWw&redir_esc=y#v=onepage&q&f=false
[7] A. Wörz, K. Wudy, D. Drummer, A. Wegner, and G. Witt, "Comparison of long-term properties of laser sintered and injection molded polyamide 12 parts," *Journal of Polymer Engineering*, vol. 38, no. 6, pp. 573–582, 2018, doi: 10.1515/polyeng-2017-0227.
[8] C. Klahn, *Laseradditiv gefertigte, luftdurchlässige Mesostrukturen*. Berlin, Heidelberg: Springer Berlin Heidelberg, 2015.
[9] G. A. O. Adam, "Systematische Erarbeitung von Konstruktionsregeln für die additiven Fertigungsverfahren Lasersintern, Laserschmelzen und Fused Deposition Modeling," Dissertation, Universität Paderborn, Paderborn, 2015.
[10] *Kunststoffe – Prüfverfahren zur Bestimmung des Verhaltens gegen flüssige Chemikalien*, 175, DIN EN ISO, Berlin, 2011.
[11] *Kunststoffe - Bestimmung der Zugeigenschaften*, 527, DIN EN ISO, Berlin, 2019.
[12] *Kunststoffe - Bestimmung der Charpy-Schlageigenschaften*, 179, DIN EN ISO, Berlin, 2000.
[13] BASF, *GLYSANTIN® G40®: Datenblatt.* [Online]. Available: https://www.glysantin.de/glysantinr-g40r-konzentrat (accessed: May 19 2021).
[14] ZELLER + GMELIN, *Divinol Spezialöl HGB.* [Online]. Available: https://www.zeller-gmelin.de/zgSite/de/Lubricants/Bau/Getriebe%C3%B6l-Nutzfahrzeuge/Divinol-Spezial%C3%B6l-HGB/p/51880?s=6C9AAA14BAC4711593BD45A9E8D598C35672E580 (accessed: May 19 2021).
[15] BASF, *Technical Data Sheet Ultrasint® PP nat 01.* [Online]. Available: https://forward-am.com/material-portfolio/ultrasint-powders-for-powder-bed-fusion-pbf/pp-line/ultrasint-pp-nat-01/ (accessed: May 19 2021).
[16] C. Kummert, W. Diekmann, K. Tews, and H.-J. Schmied, "Influence of Part Microstructure on mechanical Properties of PA6X Laser Sintered Specimens," in *Solid Freeform Fabrication 2019 - Proceedings*, Laboratory for Freeform Fabrication and University of Texas at Austin, Ed., 2019, pp. 735–744.
[17] *Zerstörungsfreie Prüfung: Dichtigkeitsprüfung: Kriterien zur Auswahl von Prüfmethoden und -verfahren*, 1779, DIN, Berlin, 1999.
[18] *Prüfung von Kunststoffen - Bestimmung der Gasdurchlässigkeit: Teil 2: Manometrisches Verfahren zur Messung an Kunststofffolien*, 53380-2, DIN, Berlin, 2006.
[19] A. Folger and L. Erdt, *STATE-OF-THE-ART SURFACING STATE-OF-THE-ART SURFACING - EIN ÜBERBLICK FÜHRENDER VERFAHREN FÜR SLS & MJF BAUTEILE.* [Online]. Available: https://dyemansion.com/wp-content/uploads/2019/12/dyemansion_state-of-the-art-surfacing-whitepaper_11-19_de.pdf (accessed: Mar. 19 2021).